Type IV creep crack initiation and propagation in mod.9Cr-1Mo steel welds

Takashi Honda[1*], Takuya Fukahori[1], Takumi Tokiyoshi[1], Toshihide Igari[1], Kimihiko Tominaga[2] and Alan CF. Cocks[3]

[1]Research and Innovation Center, Mitsubishi Heavy Industries, Ltd., Nagasaki851-0392, Japan
[2]Boiler Engineering Department, Mitsubishi Heavy Industries , Ltd., Yokohama2208401, Japan
[3]Department of Engineering Science, University of Oxford, Parks Road, OX1 3PJ, UK
* takashi.honda.yd@mhi.com

Summary
The ratio of crack initiation and crack propagation life is important from the viewpoint of residual life prediction of mod. 9Cr-1Mo steel welds under Type IV creep damage. Both the creep void density distribution and the failure process with crack initiation/propagation/final failure are predicted for three types of welds in pipes and nozzles, which are compared with experimental results at 650˚C. The ratio of crack initiation and final failure life depends on weld type and loading conditions; the ratio is about 0.95 in the cases where redistribution of stress occurs only in the thickness; the ratio is 0.59~0.65 in the cases where redistribution of stress occurs in both the thickness and circumferential directions of the pipe. Influence of stress ratio (axial vs. circumferential stress) is also predicted for circumferential welds subject to internal pressure / axial load and is compared with experimental results at 650˚C.

Key Words
Creep damage, Type IV, mod. 9Cr-1Mo steel, welded joint, crack initiation, crack propagation.

Introduction
Creep strength of welded joints in power piping, such as similar and dissimilar metal welds, is a key to confirming structural reliability in long-term operation of USC (ultra-supercritical) power plants using modified 9Cr-1Mo steel (ASME P91). Both Type IV creep failure [1] in similar metal welds and interface failure [2, 3] in dissimilar metal welds of P91/Inconel are considered in the design stage and in residual life predictions at high temperatures. Since creep strength reduction in similar metal welds of mod.9Cr-1Mo steel in long-term creep [4] was confirmed experimentally, residual life prediction for Type IV creep failure has been an important theme in Ultra Super Critical (USC) plants after long-term service.
From a metallurgical point of view [5], the high-creep strength of mod.9Cr-1Mo steel is due to the various strengthening mechanisms against creep deformation. However, these mechanisms are gradually diminished due to microstructural changes during long-term creep, such as a decrease in the number density of precipitates ($M_{23}C_6$ etc.) accompanying an increase in their size; and an increase in the size of lath-martensitic microstructures. As a result of the welding process and subsequent PWHT, the edge of the heat-affected zone (HAZ) adjacent to the base metal, known as the fine-grained HAZ (FGHAZ), develops an equiaxial fine-grained structure with low hardness and low creep strength. According to the microscopic observation of the nucleation process of creep voids in the FGHAZ of modified 9Cr-1Mo steel by Masuyama et al. [6], creep cavities of submicron size nucleate at precipitates, at triple points, or grain boundaries of 5μm-size grains, after which they grow and coalesce. They then surround the grain, resulting in the formation of defects (voids) of the order of the grain size, which connect with adjacent defects (voids), to form micro-cracks. The increase in the number density of grain size defects (voids) is used as an index of actual creep damage [7].
A damage-mechanics approach [8-11] seems to be appropriate for simulating the failure process from microscopic damage of the FGHAZ to final fracture of a welded joint. However, the correspondence between the damage variable and the number density of creep voids (creep void density in brevity), i.e., the physical meaning of the damage variable, has not been sufficiently examined. Fukahori et al. [12, 13] carried out damage simulations of large-uniaxial cross welds using a random-fracture-resistance model of grain boundaries (random-fracture-resistance model in brevity), which can express initiation and coalescence of defects (voids) of the order of the grain size. Creep void density distributions in the large-uniaxial cross welds was predicted with the help of stress distributions determined from FE creep analyses, and final rupture life was also predicted using a damage mechanics concept.
Honda et al. [14, 15] developed a damage simulation method combining continuum damage mechanics and a void nucleation model (void mechanics model) proposed by Gonzalez and Cocks [16] in which a grain-size cavity formed by failure of all its facets under a multiaxial stress state is regarded as a void. The merit of this method is to be able to predict both creep void density and rupture life of welded structures at the same time.
From a damage-mechanics point of view, the mechanism of Type IV creep failure within the FGHAZ is composed of two stages [14, 15]: a stage of increasing creep void density with a size comparable to the FGHAZ grain size (5μm); and a strain softening stage in the last part of creep life.

In this paper, a creep damage analysis scheme considering the above two mechanisms is applied to welded joints with non-uniform weld metal materials, HAZ and base metal, such as those found in large uniaxial cross-weld specimens. A void-mechanics model [16] expresses the increase of creep void density in terms of a strain for void nucleation, which is strongly influenced by the multiaxial state of stress. A critical value of creep void density corresponding to initiation of a micro-crack has been determined based on the results of the random-fracture-resistance model [13] by the authors of this paper.
Both the creep void density distribution and the failure process with crack initiation, propagation and final failure are predicted by the analysis, and are compared with experimental results at 650˚C for three types of welds: a longitudinal weld, a circumferential weld and a nozzle junction weld. Influence of stress ratio (axial vs. circumferential stress) is also predicted for circumferential welds subject to internal pressure/axial load and compared with experimental results at 650˚C.

Outline of damage analysis

Since void nucleation and damage models for the FGHAZ have been reported in a previous paper [14, 15], only an outline is given here. A creep constitutive law of the FGHAZ was formulated based on the model of Perrin-Hayhurst [17] as shown in eq. (1), which considers both mechanical damage due to creep voids and metallurgical damage by strain softening.

$$\dot{\varepsilon}_{ij}^{c} = \frac{3}{2} A \sinh\left[\frac{B\sigma_{eq}}{(1-G)(1-D)}\right] \frac{\sigma_{ij}^{D}}{\sigma_{eq}} \qquad (1)$$

where σ_{ij}^{D} , σ_{eq} , G , D , A and B are respectively deviatoric stress, von Mises equivalent stress , damage parameter due to strain softening, damage parameter associated with creep voids and two material constants. In this equation, primary creep is neglected, but both secondary and tertiary creep due to damage development and strain softening are considered. The evolution equation for damage G is expressed as eq. (2), where the first term is due to strain softening and depends on the von Mises equivalent creep strain rate $\dot{\varepsilon}_{eq}^{c}$ and yield stress σ_y; the second term is the time dependent thermal softening; and α , κ and Kc are material constants. Material constants in eq. (1) and (2) are determined using uniaxial creep data.

$$\dot{G} = \alpha \left(\frac{\sigma_{eq}}{\sigma_y}\right)^{\kappa} \dot{\varepsilon}_{eq}^{c} (1-G)^2 + \frac{Kc}{3}(1-G)^4 \qquad (2)$$

The damage parameter D due to creep voids is defined by eq. (3) in relation to the creep void area density N (1/mm^2).

$$D = \frac{N}{40000} \qquad (3)$$

The denominator in eq. (3) is the total number of grains in 1 mm^2 for an average grain size of 5μm. This number (40000) is derived from reference [13]. The void nucleation model in eq. (4) was proposed by Gonzalez and Cocks [16] as a model applicable to the FGHAZ of P91 under a multiaxial state of stress. In eq. (4), the void nucleation rate $\dot{N}$ is a function of the creep strain rate and tri-axiality factor X in eq. (5), where σ_m is the hydrostatic stress, defined by the sum of the three principal stresses divided by three.

$$\dot{N} = a\, \dot{\varepsilon}_{eq}^{c} \left(\frac{4}{9} + \frac{20}{9} X^2\right) \qquad (4)$$

$$X = \frac{3\sigma_m}{2\sigma_{eq}} \qquad (5)$$

Different from uniaxial creep, where ductile failure is found, multi-axial creep, as in Type IV failure, exhibits a brittle failure mode, arising from the nucleation, growth and coalescence of creep voids forming micro-cracks, which interlink leading to final failure. The critical damage D_{cr} corresponds to the initiation of a micro-crack resulting from the coalescence of voids. Based on the comparison of microscopic observations and simulation results by the random-fracture-resistance model [13], N=4000/mm^2 is adopted as a critical value for the formation of micro-cracks. The critical damage D_{cr} is then determined as “0.1”.

Background of determining the critical value for the formation of micro-cracks is described in detail. As shown in Fig.1 [13], Fukahori et al. carried out a simulation using the random-fracture-resistance model and compared with observation results [7] of the large-uniaxial cross weld (Case 1 in the next section). The concept of this model is to consider a grain boundary having a random length and an initial fracture resistance. The resistance reduces by the product of a fracture driving force and time, and the grain boundary becomes defect (void) when the resistance becomes zero. The fracture driving force was separately determined from three kinds of tests. Firstly, the randomness of the fracture resistance was set so that the measurement results for the time history of the creep void density could be expressed. In the case of Fig.1, ten observation points along the FGHAZ line in the width of the top surface (Location A in Fig.1) were selected for this purpose. The scatter of these ten points could be expressed using the ten times of Monte-Carlo simulation varying grain boundary length and initial fracture resistance. Then the creep void distribution in the joint section in the figure was predicted; the variation in the prediction is the result of ten times of Monte-Carlo simulation; observation results for creep void density was obtained from the opposite side of the fractured specimen; a crack was observed in the vicinity of 2 mm from the top surface; and the creep void density at this location was 2500~4000/mm^2. Here, N = 4000/mm^2 was selected as an index of micro-crack initiation. In the case of 4000/mm^2, the critical damage D_{cr} is 0.1 (=4000/40000), but in the case of 2500/mm^2, D_{cr} is 0.06. It is noted that the prediction of the crack initiation life varies depending on the definition of D_{cr}.

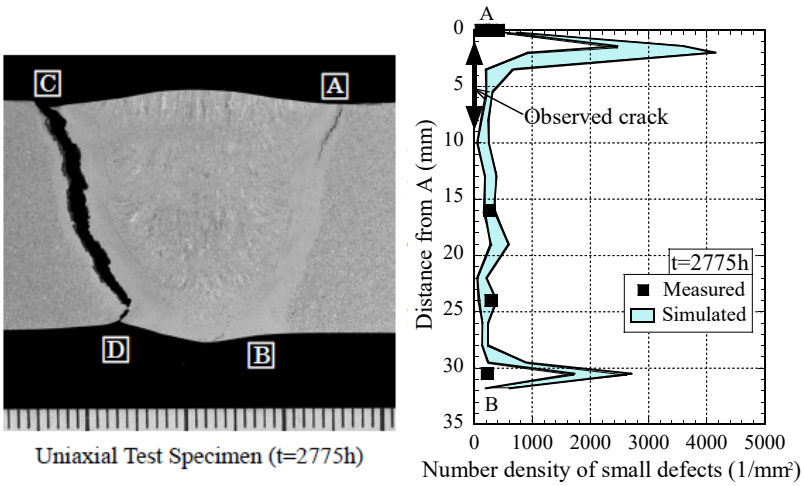

Figure 1 Analysis results of large-uniaxial cross weld (Case 1) [13].

With respect to the determining process of the constant “a” in eq. (4), some explanation is added referring to the results of our work [14]. Fig. 2 shows the observation results of voids in two kinds of creep rupture specimen of simulated-FGHAZ of mod. 9Cr-1Mo steel [14]. The specimen was a double-notch specimen, and the other side of the ruptured notch was observed after the test. In the sharp notch, a large number of voids were observed near the bottom of the notch, while in the blunt notch a large number of voids were observed in the center of the specimen. Fig. 3 shows comparison of the simulation and observation results of the creep void distribution at the notch root section. The simulation based on eq. (4), in which the stress multiaxiality and creep strain rate are considered, could express the creep void distribution of the two types of notched specimen. Although the calibration of the constant “a” was performed to match the peak of the void density (around 2400/mm^2) of sharp notch, simulation results are found to reproduce the experimentally-obtained creep void distributions in the two kinds of notch acuities.

Young’s modulus reduces depending on the progress of creep void density [18] as shown in eq (6).

$$E = E_0\left(1 - \frac{D}{D_{cr}}\right) \qquad (6)$$

where E and E_0 are Young’s modulus of damaged and non-damaged material, respectively.

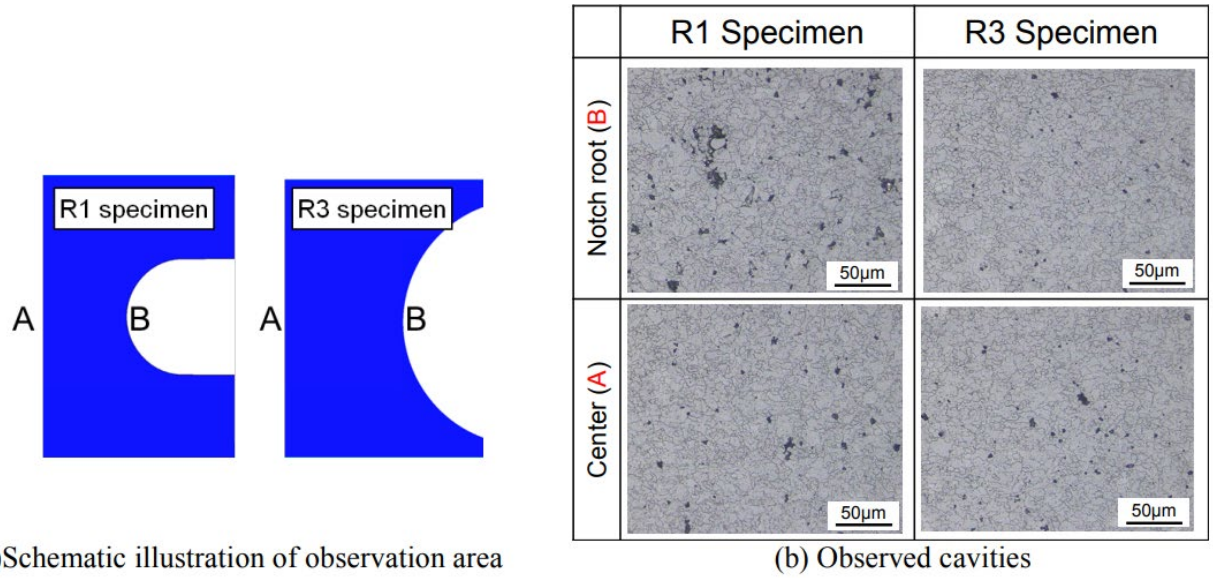

Figure 2 Observed voids at several locations in the notched specimens. [14].

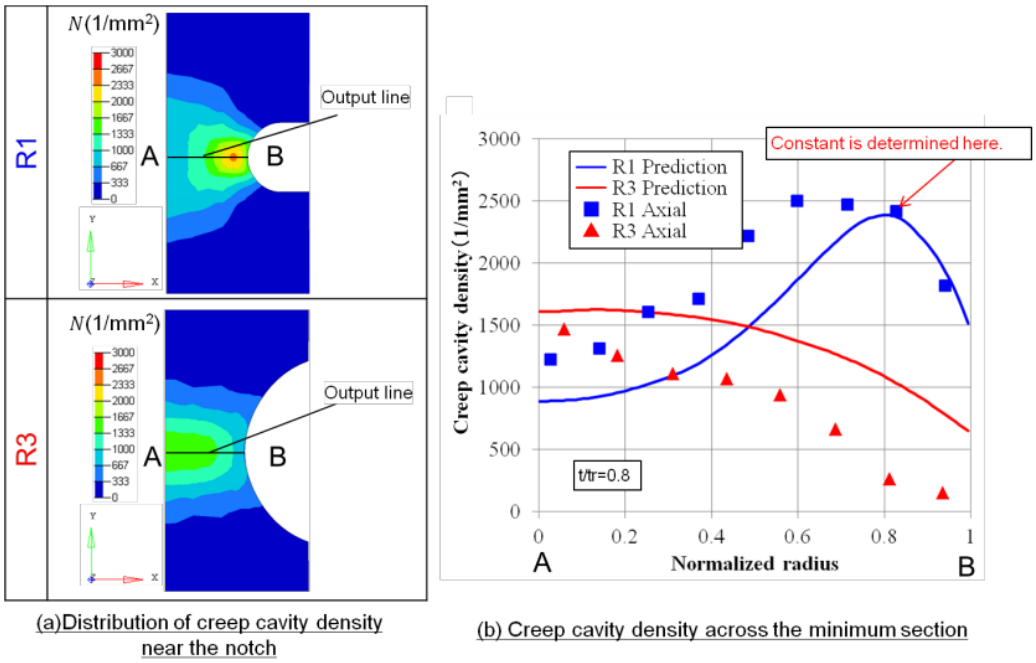

Figure 3 Creep void density distribution in notched specimens from damage analysis [14].

Damage analysis of various weld configuration

Both the creep void density distribution and the failure process with crack initiation, propagation and final rupture were predicted by the analysis for the following four cases. Analysis results for Cases 1-3 were compared with existing experimental results. Continuous observation from microscopic damage to macroscopic crack initiation/propagation is usually difficult in the experiment for Type IV damage. With respect to the measurement of damage in experiments, creep void density was measured at the end of the test in Case 1 [7]; observation of creep void was not performed but final rupture life was observed in Case 2 [20]; existence of crack-like damage at the mid-wall thickness was predicted by phased array ultrasonic test (PAUT) in the middle of the test and cracks were observed after the test in Case 3 [19]. FE models for the four cases consist of base metal, weld metal and FGHAZ. The creep constitutive law of the FGHAZ is given in eq. (1), showing secondary and tertiary creep due to strain

softening and damage; the creep law for the base metal and weld metal are the same Blackburn type equation, showing primary and secondary creep [15].
During creep, stress re-distribution in the welded joints occurs due to the progress of creep strain and damage.
In the FEM analysis, crack initiation life was defined as the time when the creep void density of some FEM elements reaches N=4000/mm^2 (Dc = 0.1); crack propagation was defined as a coalescence of FEM elements reaching N=4000/mm^2 and losing rigidity; and final failure was defined as a time when the macroscopic creep strain rate becomes infinite as a result of a continuous region of FGHAZ losing rigidity.
Case 1 is a large-uniaxial cross weld simulating an actual longitudinal welded pipe with U-shaped weld configuration of w42mm x t32mm under a nominal stress of 66MPa at 650˚C. In the actual components, applied stress is near the allowable stress at around 600˚C. To obtain a realistic rupture time in the test, there are two methods; one is increasing stress level at 600˚C; and the other is keeping stress level and increasing temperature up to 650˚C. The former approach often results in ductile rather than brittle failure found in Type IV damage. The latter approach, on the other hand, can reproduce the failure mode of Type IV damage. We adopted the latter method to obtain a realistic rupture life with keeping the failure mode. The commercial FEM code ABAQUS (ver. 6.12-2) and the generalized plane strain element (CPEG4R and CPEG3) were used; and there are four elements across the width (approximately 2 mm) of the FGHAZ region. Figure 4 [15] depicts the distribution of creep void density at both crack initiation and final failure. Black indicates a cracked area with creep void density over 4000/mm^2. Distribution of creep void density changes as time progresses, reflecting the re-distribution of stress through the thickness. Predicted crack initiation and rupture time by creep damage analysis were 4825 h and 5100h, within a factor of 2 on life when compared with the experimental rupture life of 2775.2h [15].
Case 2 is a circumferentially welded tube subject to internal pressure and axial load at 650˚C. Details of experimental and predicted results are shown later in the next section.
Case 3 is a circumferentially welded pipe of OD686mm x t30mm subject to an internal pressure of 3.9MPa and four-point bending (elastic bending stress 36.8MPa) at 650˚C. A hexahedral solid element C3D8RH and a triangular-prism solid element C3D6H in the commercial code ABAQUS (ver.6.12-2) were employed together with symmetry boundary conditions. The HAZ in the model consists of two areas; a “hardened HAZ” with 2 mm width (four-element layers) and a “softened HAZ” with 2 mm width (four-element layers). In this paper, the four-element layers of the softened HAZ were regarded as the FGHAZ. Figure 5 [15] depicts the distribution of creep void density at both crack initiation and final failure. Different from the longitudinal weld (Case 1), re-distribution of stress is found in both the thickness and circumferential directions of the pipe. Crack propagation takes longer when compared with longitudinal welds. Predicted lives of crack initiation and final failure were 3250 h and 4970h, against experimentally obtained lives of 3500h and 6930h [15].
Case 4 is a nozzle junction weld with a configuration consisting of a main pipe of OD368.3mm x t78mm and stub of OD45mm x t12mm under an internal pressure of 34.2MPa at 650˚C (See Fig. 6). FEM code and type of element are the same as Case3; and there are three elements across the width (3mm) of the FGHAZ. Figure 7 depicts the creep void density distribution on the FGHAZ surface neighbouring base metal at crack initiation and final failure. Similar to Case 3 (circumferential weld), re-distribution of stress is found in both thickness and circumferential directions of the pipe. Crack propagation takes longer time when compared with longitudinal welds. Only damage analysis results are presented for this case. The creep void density and circumferential stress distributions at crack initiation and final failure are shown in Fig. 7 and Fig. 8, respectively. Compared with the longitudinal weld in which the stress is uniform in the cross section, the circumferential weld has a longer propagation time because the damage propagates in both the thickness and circumferential directions. The ratios of crack initiation and final failure life for Cases 1-4 are shown in Fig. 9. For the circumferential weld subject to internal pressure / axial bending (Case 3) and the nozzle junction weld subject to internal pressure (Case 4), the ratios of crack initiation and final failure life were 0.65 (Case 3) and 0.59 (Case 4). The reason for a lower ratio than that for Cases 1 is that redistribution of stress can occur in both the thickness and circumferential directions of the pipe. Crack penetration in the thickness direction was delayed due to the influence of re-distribution of stress along the circumference of the pipe.

Influence of biaxial stress ratio on failure life of circumferential welds

The outer diameter and thickness of the circumferentially-welded-tube specimens were 36 and 6 mm, respectively. Tests were carried out at 650 °C by applying internal pressure by means of steam and axial load using nitrogen gas. The test parameter of interest here is the macroscopic stress ratio (σ_z/σ_θ). An example of the experimental results [20] is shown in Fig.10. Along with an increase of stress ratio, the failure pattern was changed from base metal failure to FGHAZ failure.
Creep damage analysis was applied to predict crack initiation and final failure life. Fig. 11 shows an example of the analysis results for crack initiation and final failure for a stress ratio of 1.2. The FEM model is an axisymmetric model for ABAQUS ver6.12-2, consisting of base metal, FGHAZ and weld metal; and there are six elements (CAX4) across the width (4.0 ~ 4.7mm) of the FGHAZ. The crack initiation life was 95% of final failure. Different from the

circumferential weld in the last section, redistribution of stress occurred only through the thickness of the specimen; this is the reason why the ratio of crack initiation and final failure was almost equal to that of the longitudinal weld. The results are summarized in Fig.12, comparing experimental and predicted failure life. Final failure lives in the experiment were predicted well by the analysis. In the figure, two failure modes (Base metal failure and FGHAZ failure) are presented by bold lines following Himeno et al. [20].
In the cases of circumferential welds subject to internal pressure / axial load (Case 2) and longitudinal welds (Case 1), the ratio of crack initiation and final failure life was almost the same, about 0.95. The reason for this result is that redistribution of stress can occur only through the thickness in both cases.

Concluding remarks

Results are summarized as follows.

1. In the longitudinal welds (Case 1) and circumferential welds subject to internal pressure / axial load (Case 2), the ratio of crack initiation and final failure life was almost the same, about 0.95. The reason for this result is that redistribution of stress can occur only in the thickness in both cases.
2. In the circumferential weld subject to internal pressure/axial bending (Case 3) and nozzle junction weld subject to internal pressure (Case 4), the ratios of crack initiation and final failure life were 0.65 (Case 3) and 0.59 (Case 4). The reason for the lower ratio than that for Cases 1 & 2 is that redistribution of stress can occur in both thickness and circumferential directions of the pipe. Crack penetration through the thickness was delayed due to the influence of redistribution of stress in the circumference of the pipe.
3. In the circumferential weld subject to internal pressure/axial bending (Case3) & nozzle junction weld (Case 4), there is an opportunity to propose countermeasure because the low ratio of crack initiation and final failure life.

References

[1] F. Masuyama, “Creep degradation in welds of mod. 9Cr-1Mo steel”, Int. J. Pressure Vessels and Piping, Vol.83, Issue 11-12 (2006) pp.819-825. https://doi.org/10.1016/j.ijpvp.2006.08.010.
[2] J. Hu, T. Fukahori, T. Igari, Y. Chuman, ACF. Cocks, “Modelling of creep rupture of ferritic/austenitic dissimilar weld interfaces under mode I fracture”, Engineering Fracture Mechanics, Vol.191 (2018) pp.344-364. https://doi.org/10.1016/j.engfracmech.2018.01.001.
[3] J. Hu, E.Elmukashfi, T. Fukahori, T. Igari,Y. Chuman, ACF. Cocks, “Effect of weld angle on the creep rupture life of ferritic/austenitic dissimilar weld interfaces under remote mode I fracture”, Engineering Fracture Mechanics, Vol.218, 106606 (2019). https://doi.org/10.1016/j.engfracmech.2019.106606.
[4] M. Tabuchi and Y. Takahashi, “Evaluation of creep strength reduction factors for welded joints of modified 9Cr-1Mo steel (P91)”, ASME 2006 Pressure Vessels and Piping/ICPVT-11 Conference, Volume 6: Materials and Fabrication, Vancouver, BC, Canada, July 23–27 (2006). https://doi.org/10.1115/PVP2006-ICPVT-11-93350.
[5] K. Arisue, N. Komai, K. Tominaga, M. Fujita, “Microstructures of fine-grained HAZ and long-term creep rupture strength in mod.9Cr-1Mo steel weldments”, 4th International Creep Conference ECCC (2017).
[6] F. Masuyama and T. Yamaguchi, “Creep damage initiation mechanism and life of martensitic structures”, Proc. of 51st Symposium on High-Temperature Strength of Materials, pp.110-114 (2013).
[7] N. Komai, T. Tokiyoshi, T. Igari, H. Ohyama, F. Masuyama and K. Kimura, “Experimental observation of creep damage evolution in seam-welded elbows of mod. 9Cr-1Mo steel”, Materials at High Temperatures vol.33, Issue 6 (2016) pp.615-625. https://doi.org/10.1080/09603409.2016.1204063.
[8] ST. Tu, P. Segle and JM. Gong, “Creep damage and fracture of weldments at high temperature”, Int. J. Pressure Vessels and Piping, Vol.81, Issue 2 (2004) pp.199-209. https://doi.org/10.1016/j.ijpvp.2003.11.010.
[9] TH. Hyde, W. Sun and JA.Williams, “Creep analysis of pressurized circumferential pipe weldments - A review”, J Strain Analysis, Vol.38, No.1(2004) pp.1-29. https://doi.org/10.1115/PVP2016-63355.
[10] M. Yatomi, AD. Bettinson, NP. O′Dowd, KM. Nikbin, “Modelling of damage development and failure in notched bar multiaxial creep tests”, Fatigue & Fracture of Engineering Materials & Structures, Vol.27 (2004) pp.283-295. https://doi.org/10.1111/j.1460-2695.2004.00755.x.
[11] H. Hongo, M. Tabuchi, Y. Li, Y. Takahashi, “Creep damage behavior of Mod.9Cr-1Mo steel welded joint”, J. The Japan Society of Materials Science, Japan, Vol.58, No.2 (2009) pp.101-107. https://doi.org/10.2472/jsms.58.101.
[12] T. Igari, T. Fukahori, F. Kawashima, T. Tokiyoshi, Y. Chuman, N. Komai, M. Fujita, “Micro-macro creep damage simulation for welded joints”, Materials at High Temperatures, Vol.28, No.3 (2011) pp.181-187. http://dx.doi.org/10.3184/096034011X13123545763673.
[13] T. Fukahori, T. Tokiyoshi, T. Igari, Y. Chuman and N. Komai, “Prediction of Type-IV creep failure of a seam-welded mod. 9Cr-1Mo elbow based on microscopic damage simulation”, Materials at High Temperatures, Vol.34, Issue 3 (2017) pp.194-207. https://doi.org/10.1080/09603409.2017.1289621.

[14] T. Honda, T. Fukahori, T. Igari, Y. Chuman, T. Tokiyoshi and ACF. Cocks, “Creep damage analysis of simulated-HAZ notched bar specimens of modified 9Cr-1Mo steel”, JSME Mechanical Engineering Journal, Vol. 4, No. 5 (2017) pp.1-13. https://doi.org/10.1299/mej.16-00697.
[15] T. Honda, T. Fukahori, T. Tokiyoshi, Y. Chuman, T. Igari and ACF. Cocks, “Creep damage analysis of mod.9Cr-1Mo steel welds considering void mechanics modelling”, International Journal of Pressure Vessels and Piping, Vol.189 (2021),104251. https://doi.org/10.1016/j.ijpvp.2020.104251
[16] D. Gonzalez, ACF. Cocks, T. Fukahori, T. Igari and Y. Chuman, “Creep failure of a P91 simulated heat affected zone material under multiaxial state of stress”, Proc. 3rd Intern. ECCC Conf. on Creep & Fracture (2014).
[17] IJ. Perrin, and DR. Hayhurst, “Continuum damage mechanics analyses of type IV creep failure in ferritic steel crossweld specimens”, International Journal of Pressure Vessels and Piping, Vol.76, Issue 9 (1999) pp.599-617. https://doi.org/10.1016/S0308-0161(99)00051-4.
[18] Lemaitre J., “A continuum damage mechanics model for ductile fracture”, Trans ASME J. Eng. Mater. Technol.Vol.107(1985), pp.83–89. https://doi.org/10.1115/1.3225775
[19] S. Nishinoiri, Y. Takahashi, H. Fukutomi and M. Yaguchi, “Inner pressure/bending creep test on circumferentially welded large diameter pipe of Grade 91 steel: Creep Damage Mechanism and Applicability of NDE”, Proc. ASME PVP2016, Vancouver, Canada, PVP2016-63176 (2016). https://doi.org/10.1115/PVP2016-63176.
[20] T. Himeno, Y. Chuman, T. Tokiyoshi, T. Fukahori, T. Igari, “Creep rupture behavior of mod. 9Cr-1Mo steel pipe subject to internal pressure and axial load”, Materials at High Temperatures, Vol.33, Issue 6 (2016) pp.636-643. https://doi.org/10.1080/09603409.2016.1226703.

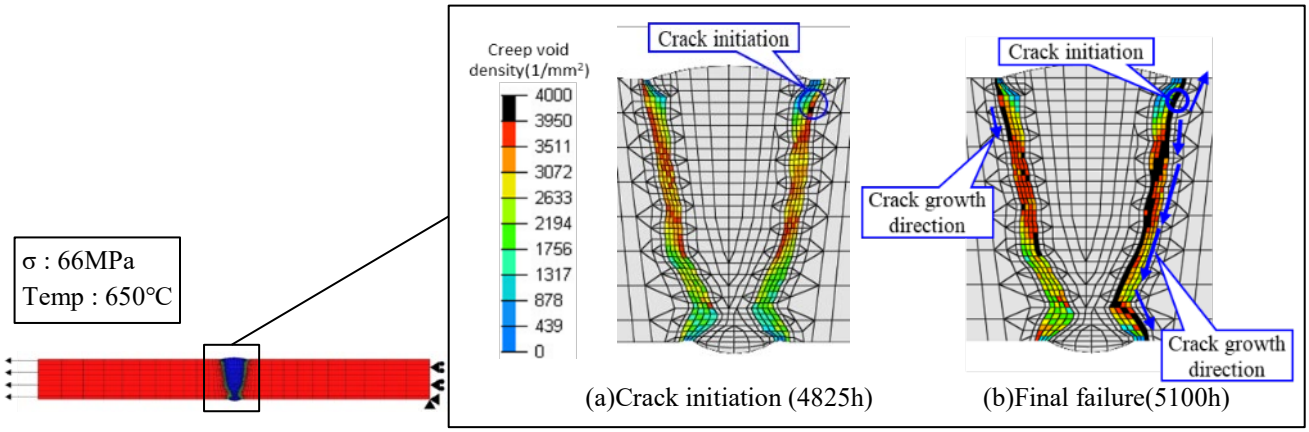

Figure 4 Analysis results of longitudinal weld (Case 1) [15].

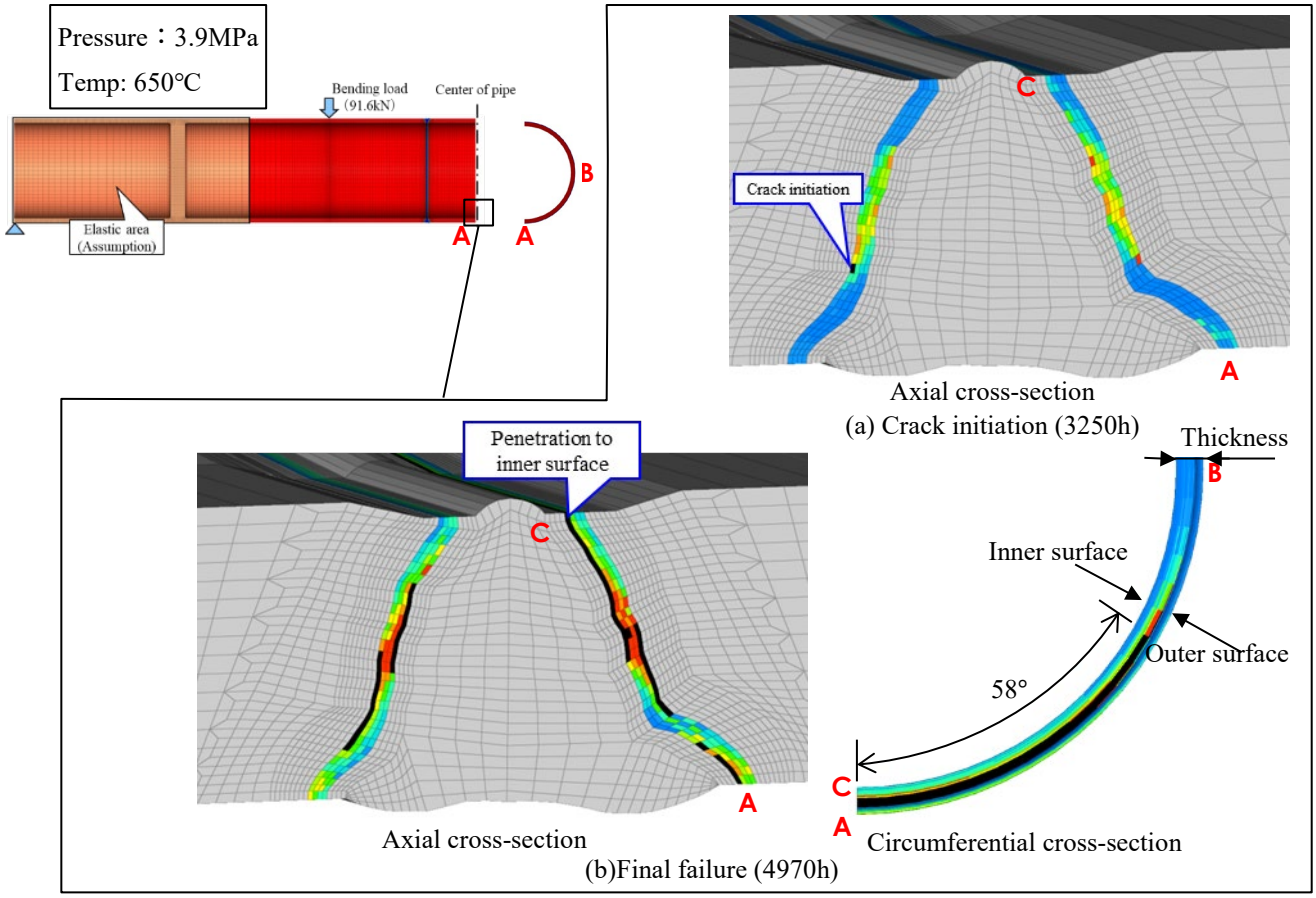

Figure 5 Analysis results of circumference weld (Case 3) [15].

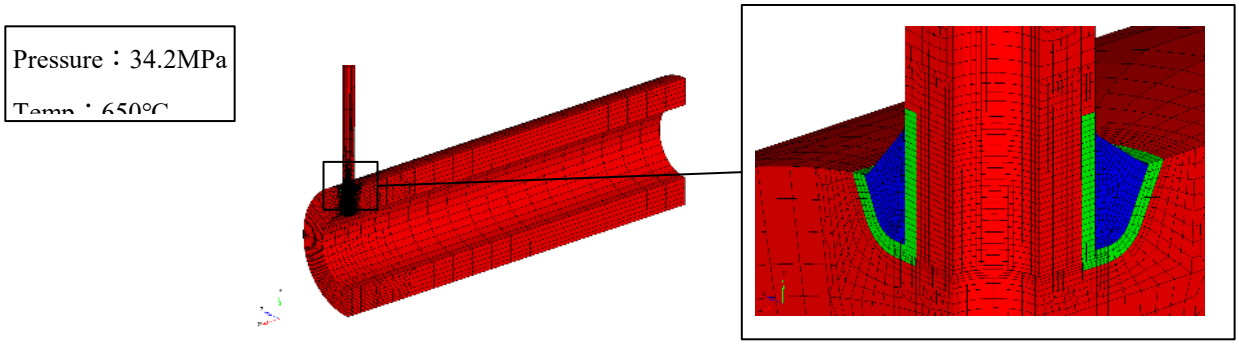

Figure 6 Analysis model of nozzle junction weld (Case 4).

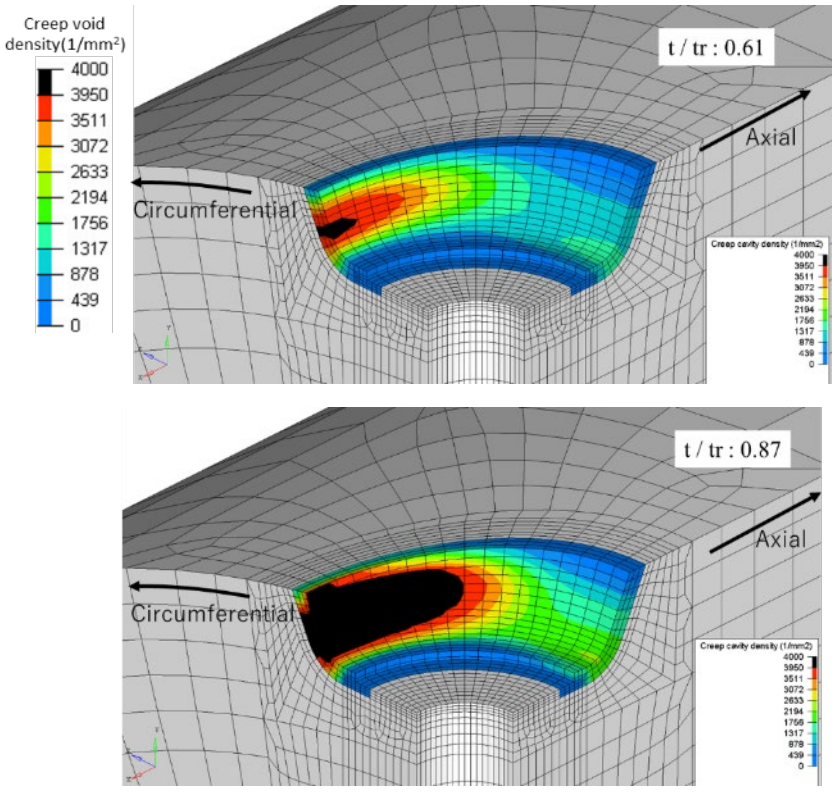

Figure 7 Creep void density distribution on FGHAZ surface of nozzle junction weld (Case 4) after creep.

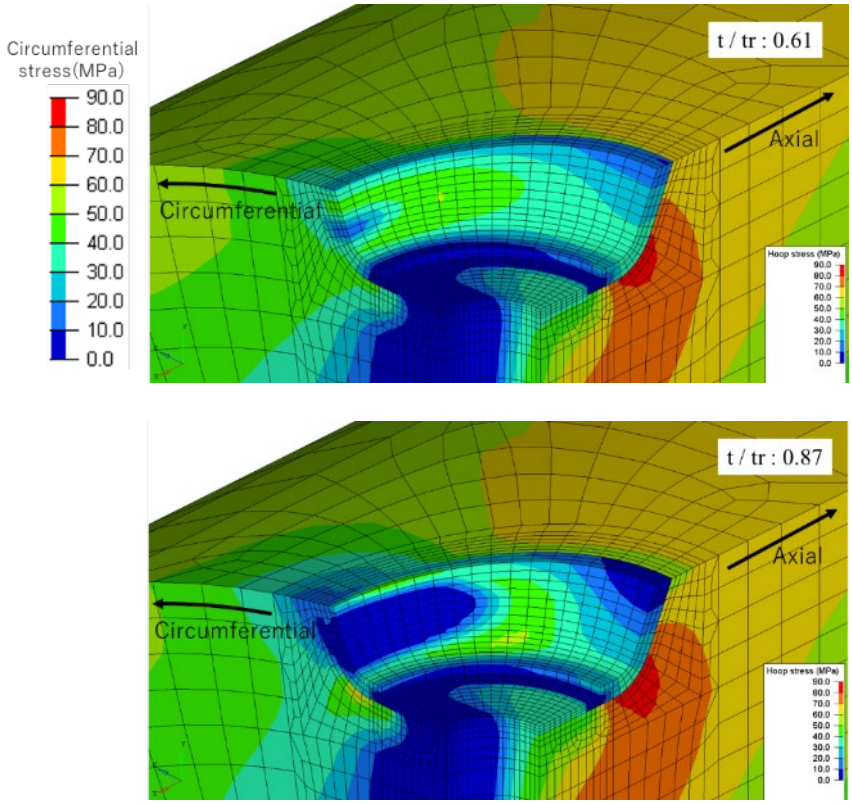

Figure 8 Circumferential stress distribution on FGHAZ surface of nozzle junction weld (Case 4) after creep.

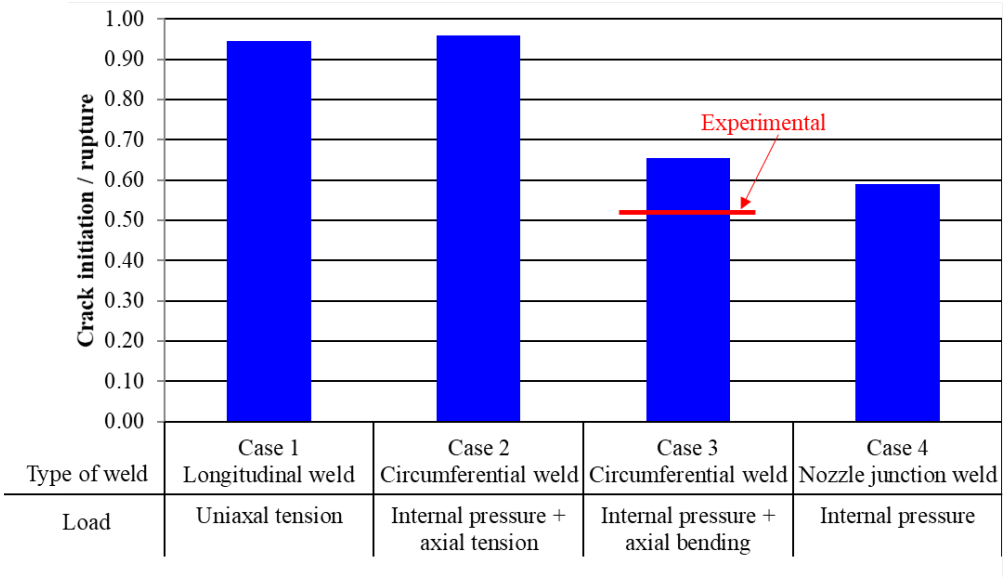

Figure 9 Ratio of crack initiation and rupture time.

	Internal pressure only	Internal pressure and axial load		Axial load only
Morphology				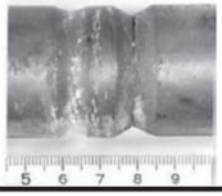
Macroscopic stress ratio σ_z/σ_θ	0.5	0.8	1	∞
Crack direction	Axial	Circumferential	Circumferential	Circumferential
Crack location	Base metal	FGHAZ	FGHAZ	FGHAZ

Figure 10 Creep rupture morphology for different stress ratios σ_z/σ_θ [20].

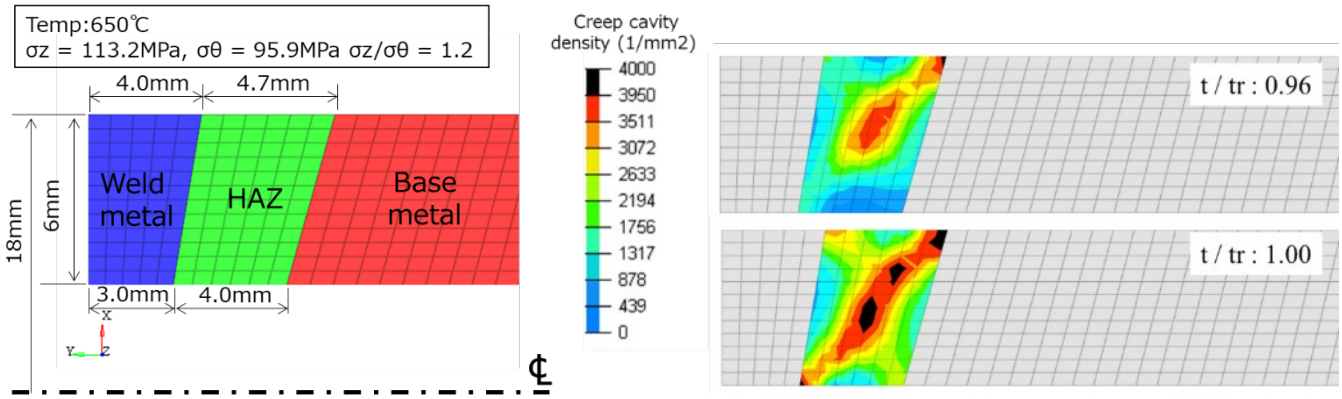

Figure 11 Creep void density distribution of circumferential weld under internal pressure and axial load (Case 2).

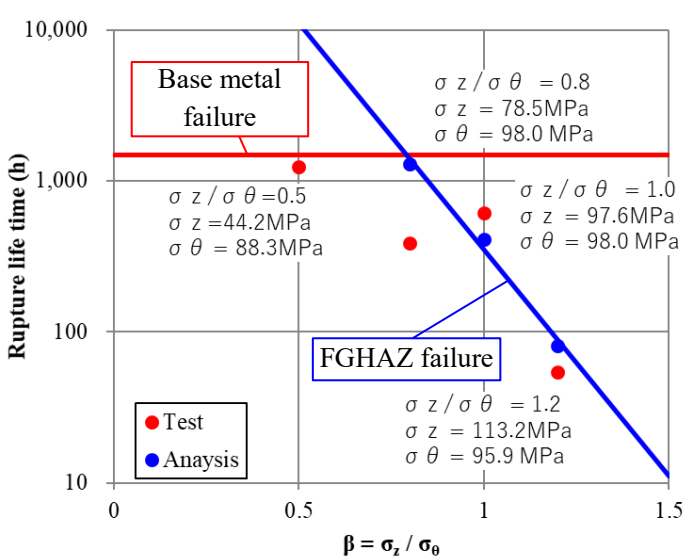

Figure 12 Relationship between creep rupture life and stress ratio under internal pressure and axial load (Case 2)